Heberle, ANA.; García Gabaldón, M.; Ortega, EM.; Bernardes, AM.; Pérez-Herranz, V. (12-2). Study of the atenolol degradation using a Nb/BDD electrode in a filter-press reactor. Chemosphere. 236:1-8. https://doi.org/10.1016/j.chemosphere.2019.07.049

Study of the atenolol degradation using a Nb/BDD electrode in a filter-press reactor

Alan Nelson Arenhart Heberle[a,b], Montserrat García-Gabaldón[a], Emma María Ortega[a], Andréa Moura Bernardes[b], Valentín Pérez-Herranz[a*]

[a] Grupo IEC, Departamento de Ingeniería Química y Nuclear, E.T.S.I. Industriales, Universitat Politècnica de València, P.O. Box 22012, E-46071, Valencia, Spain

[b] Universidade Federal do Rio Grande do Sul (UFRGS) – Programa de Pós-Graduação em Engenharia de Minas, Metalúrgica e de Materiais (PPGE3M), Av. Bento Gonçalves, 9500, Porto Alegre/RS, Brazil

*Corresponding author: vperez@iqn.upv.es

ABSTRACT

The present paper deals with the atenolol (ATL) degradation by advanced anodic oxidation using a boron-doped diamond anode supported on niobium (Nb/BDD). Cyclic voltammetry performed on this electrode revealed that it presents a high quality (diamond-sp^3/sp^2-carbon ratio), high potential for OER and that ATL can be oxidized directly and/or indirectly by the electrogenerated oxidants, such as hydroxyl radicals, persulfate ions and sulfate radicals.

Electrolysis experiments demonstrated that ATL degradation and mineralization follow a mixed (first and zero) order kinetics depending on the applied current density. At high applied current densities, the amount of $^{\bullet}$OH radicals is very high and the overall reaction is limited by the transport of ATL (pseudo first-order kinetics) whereas for low applied current densities, the rate of $^{\bullet}$OH radicals generation at the anode is slower than the rate of arrival of ATL molecules (pseudo-zero order kinetics). Estimated values of

k_{zero} and k_{first} based on the assumption of pseudo-zero or pseudo-first order kinetics were carried oud as a function of the supporting electrolyte concentration, indicating that both parameters increased with its concentration due the higher production of sulfate reactive species that play an important role in degradation.

Finally, MCE increased with the decrease of current density, due to the lower amount of $^{\bullet}OH$ present in solution, since this species could be rapidly wasted in parasitic reactions; and the increase of sulfate concentration due to the more efficient production of persulfate.

KEYWORDS: Advanced anodic oxidation; Atenolol; Boron doped diamond; Filter-press reactor

1 Introduction

Concern about pollutants discharge into the environment has been increased worldwide, since most of them can be persistent and/or bioaccumulative and have potential for environmental long-range transport (de Wit et al., 2019). Furthermore, some of such a chemicals are present in products daily household consumed, as personal care products, surfactants, steroid hormones and pharmaceuticals (Luo et al., 2014). The conventional water and wastewater treatments are not capable of removing these pollutants, and therefore, the substances appear in the environment having the potential to harm biota and humans (Belenguer et al., 2014; Benson et al., 2017; Baken et al., 2018). In this sense, extensive efforts have been made to develop some effective technologies able to thoroughly destroy these contaminants of emerging concern (CEC) from water.

Pharmaceutical products are widely consumed due to the wide range of medical treatments and the greater availability and access of medicines. Among them, β – Blockers such as Atenolol (ATL) are extensively employed to treat diseases of the circulatory system (Frishman, 2016). However, ATL presents a highest level of toxicity for aquatic animals and humans (Vieno et al., 2007). In EU, several monitoring campaigns studies published in last years, revealed an average concentration of ATL of approximately 4 μg L^{-1} in certain wastewaters (Sousa et al., 2018). This compound is widely used in treatments and contemplated in social programs for the provision of medicines to the population in Brazil (Ministério da Saúde, 2012). In addition, it was the best-selling drug in Brazil in 2013 (Godoy et al., 2015). Therefore, the removal of this β-Blocker before the discharge into the environment is a technological challenge.

One of the most promising methods applied to CEC abatement are the advanced oxidation processes (AOP), with special emphasis on the advanced anodic oxidation (AAO) (Kanakaraju et al., 2018). This process can promote the direct electron transfer and/or generate strong oxidative radicals, resulting in the degradation and mineralization of the organic compounds. In the direct electron transfer, the organic molecule exchanges electrons directly with the electrode surface. Additionally, in the indirect oxidation, the chemical reactions are mediated by the reactive species generated, mainly hydroxyl radical ($^{\bullet}OH$) (Panizza and Cerisola, 2009). In some cases, depending on the type of electrolyte, reactive species such as sulfate radical ($SO_4^{-\bullet}$), persulfate ions ($S_2O_8^{2-}$), active chorine speciation, active oxygen, etc. can be generated, which are either chemically/physically adsorbed on the anode surface or free in the bulk solution (Panizza and Cerisola, 2009; Radjenovic and Petrovic, 2017; Zabik et al., 2019). Such physicochemical characteristics depend on the reaction medium, operating conditions and electrode constitution (Souza et al., 2016; He et al., 2019).

In recent years, works based on different anode materials used in AAO process for CEC abatement have been reported (Mora-Gomez et al., 2018; Periyasamy and Muthuchamy, 2018; Xu et al., 2018; Kaur et al., 2019) which evaluated, their easy implementation, operation, scale-up and energy consumption (Chianca et al., 2014). One of the most promising anodes is the boron-doped diamond (BDD), due to its high capability in CEC degradation. The main advantages of this anode over other electrodes is its wide potential window, high current efficiency and its high electrochemical and corrosion stability (Panizza and Cerisola, 2005; da Silva et al., 2018). There are many papers reporting BDD-silicon supported (Si/BDD) (Polcaro et al., 2004; Ciríaco et al., 2009; Pacheco et al., 2011; Abdessamad et al., 2013) applied to CEC degradation, but

less information regarding the effect of different operational parameters on niobium substrate anodes (Nb/BDD) is available. Some studies show that the Nb/DBB anodes have effectively been used for pesticide (Dominguez et al., 2018), dyes (Clematis et al., 2017), hormones (Brocenschi et al., 2016), oil refinery effluent (Souza and Ruotolo, 2013) and some pharmaceuticals (Gutie et al., 2015) degradation.

The aim of this study is to investigate the ATL degradation by AAO using a Nb/BDD anode. The Nb/BDD anode material has been characterized by cyclic voltammetry, where parameters like the electrochemical window, oxygen evolution reaction (OER), diamond film quality (diamond-sp^3/sp^2-carbon ratio), electrogeneration of oxidants and ATL oxidation mechanism (direct and/or indirect) are studied. The influence of the concentration of sodium sulfate and current density on the ATL degradation is also evaluated.

2 Experimental

2.1 Chemicals and solutions

Atenolol active compound was purchased from Sigma–Aldrich (≥ 98%) and used for the standard solutions of the calibration curve. Na_2SO_4 used as supporting electrolyte was of analytical grade from Panreac. All solutions were prepared using distilled water.

Working solutions were made by commercial Atenolol pills diluted in distilled water, and subsequently filtered with a 2.7 μm filter paper. The conductivity of this solution was lower than the commonly used (Brillas et al., 2009). In this way, to increase the conductivity and to evaluate the effect of the supporting electrolyte on the ATL abatement, different sodium sulfate concentrations were tested: 0.014, 0.028 and 0.056 M of Na_2SO_4. The pH of the working solution was set in 9 for all experiments with NaOH 2 M, when necessary, since the pH of the post-treatment municipal wastewater is neutral or weakly basic (Atinkpahoun et al., 2018).

2.2 Electrochemical measurements

The electrochemical analysis procedures were performed using a conventional three electrode cell connected to a computer controlled potentiostat/galvanostat AUTOLAB PGSTAT302N. The reference electrode was an Ag/AgCl (3 M KCl) electrode and platinum (Pt) was employed as counter electrode. The working electrode was the Nb/BDD anode under study with a boron content of 2500 ppm (Nb/BDD_{2500}). The electrochemical experiments were performed at a scan rate of 100 mV s^{-1}. In this work, the boron content was expressed in ppm, regarding to mg kg^{-1}.

2.3 Electrochemical degradation assays

The degradation assays of the ATL were performed on a single compartment filter-press flow reactor, using flat square electrodes with a geometric surface area (A_s) of 0.01 m^2 and an electrode gap of 0.03 m. The working solution (1 L) was stored in an external reservoir and circulated through the reactor by a centrifugal pump with a flow rate of 1.67 x 10^{-5} m^3 s^{-1}. The electrochemical oxidation process was performed in galvanostatic mode and the influence of the applied current density in the range of 5, 10, 20 30 and 40 mA cm^{-2} on the ATL oxidation was tested.

2.4 Analyses

ATL degradation was assessed by a Unicam UV4-200 UV/VIS Spectrometer (using quartz cuvettes with a 10 mm optical path). The spectra obtained were in the wavelength range of 190 - 600 nm. Based on the absorption band at 274 nm, which was previously confirmed by UV/Vis, the concentration vs. absorbance curve was used to evaluate ATL decay. The mineralization was obtained by the total organic carbon (TOC) analysis, Non-Purgeable Organic Carbon (NPOC) method in a TOC-L CPH Shimadzu. Measurement of inorganic ions (NH_4^+ and NO_3^-) was performed on a Metrohm Ionic Chromatograph 883 Basic IC Plus. pH was monitored by a potentiometric method. The analyses of the intermediate compounds were performed by Multi Dimensional Gas Chromatograph–Mass Spectrometry (MDGC/GCMS) with a QP2010 ultra (Shimadzu) with the same operational parameters used by da Silva et al. (da Silva et al., 2019).

To evaluate the process efficiency, the mineralization current efficiency (MCE) was calculated (Hamza et al., 2009):

$$\mathrm{MCE}\ (\%) = \frac{\mathrm{n\ F\ V\ (TOC_0 - TOC)}}{7.2\times10^5\ \mathrm{m\ I\ t}}\ 100 \quad (1)$$

where n is the number of electrons consumed (66), F is the Faraday constant (96485 C mol^{-1}), V is the volume of the working solution (L), TOC_0 and TOC are the TOC concentrations (mg L^{-1}) at the beginning of the electrolysis and at each time respectively, 7.2 x 10^5 is a conversion factor (60 s min^{-1} x 12000 mg mol^{-1}), m is the number of carbon atoms of each ATL molecule (14), I is the applied current (A) and t is the time in minutes. The number of electrons consumed (n) was taken as 66 assuming that the overall mineralization involves the release of NH_4^+ ions according to the following reaction (Isarain-Chávez et al., 2011):

$$\mathrm{C_{14}H_{22}N_2O_3 + 25\ H_2O \rightarrow 14\ CO_2 + 2\ NH_4^+ + 64\ H^+ + 66\ e^-} \quad (2)$$

3 Results and discussion

3.1 Electrode characterization

The diamond layer quality of the BDD anode (diamond-sp^3/sp^2-carbon ratio) was measured by cyclic voltammetry in a 0.5 M H_2SO_4 solution (Watanabe et al., 2010; Einaga et al., 2014) and is presented in Fig. 1. The anode under study (Nb/BDD_{2500}) shows an important background current and a high potential for the oxygen evolution reaction (OER), indicating a relative high diamond-sp^3 content and a low carbon-sp^2 impurities at the diamond film of the anode surface. Comparing these data to previous studies (Watanabe et al., 2010; da Silva et al., 2018), same findings were obtained, ratifying the electrode quality towards sp^3-sp^2 ratio. Such an electrode characteristic is desirable in the contaminant degradation, resulting more effective the direct and/or mediated oxidation, and affecting the electrochemical oxidant generation as discussed ahead.

The generation of oxidizing radicals on the electrode surface from the supporting electrolyte or from the available ions in the reaction medium depends on the electrode diamond-sp^3/sp^2-carbon ratio (Garcia-Segura et al., 2015). To evaluate this, cyclic voltammetry was performed with the Nb/BDD_{2500} anode in a 0.014 M Na_2SO_4 solution (Fig. 1). In this figure the progressive scan to anodic direction demonstrated a shoulder (I) in the potential value of 2 V *vs.* Ag/AgCl, which represents the oxidation of the supporting electrolyte sulfate ions (SO_4^{2-}) and/or the hydrogen sulfate ions (HSO_4^-) to persulfate ones $S_2O_8^{2-}$ on the Nb/BDD_{2500} surface (Provent et al., 2004).

The $S_2O_8^{2-}$ generation can be driven basically by the adsorption of the HSO_4^- and/or SO_4^{2-} at sp^2-carbon impurities of the anode to form the sulfate radical ($SO_4^{\bullet-}$) (Davis et al., 2014); or by the indirect oxidation of the HSO_4^- and SO_4^{2-} by the hydroxyl radical

($^{\bullet}OH$) electrogenerated on the anode surface to promote $SO_4^{\bullet-}$, then reacting by pairs to give $S_2O_8^{2-}$, as shown in Eq. (3)-(7) (Serrano et al., 2002; Murugananthan et al., 2011).

$$BDD + H_2O \rightarrow BDD(^{\bullet}OH) + H^+ + e^- \quad (3)$$

$$HSO_4^- + {}^{\bullet}OH \rightarrow SO_4^{\bullet-} + H_2O \quad (4)$$

$$H_2SO_4 + {}^{\bullet}OH \rightarrow SO_4^{\bullet-} + H_3O^+ \quad (5)$$

$$2SO_4^{\bullet-} \rightarrow S_2O_8^{2-} \quad (6)$$

$$2SO_4^{2-} \rightarrow S_2O_8^{2-} + 2e^- \quad (7)$$

As already reported in the bibliography, the increase in the electrochemical generation of persulfate ions is proportional to the increase in the boron concentration. In this way, the Nb/BDD_{2500} electrode is able to produce a relative high amount of $S_2O_8^{2-}$ (da Silva et al., 2018). This increase in the $S_2O_8^{2-}$ generation can be related to the retention of sulfate species in the carbon-sp^2 impurities that have higher adsorption properties than diamond-sp^3 (Davis et al., 2014; Barreto et al., 2015) favoring the persulfate ion generation. On the other hand, the increase in the sp^3/sp^2 ratio decreases this adsorption potential, favoring the $^{\bullet}OH$ production on the diamond-sp^3 (Espinoza et al., 2018).

The Atenolol oxidation behavior on the Nb/BDD_{2500} anode was studied by cyclic voltammetry in a solution composed of 0.014 M of Na_2SO_4 and different ATN concentrations: 0.38, 0.75 and 1.13 mM. As the ATL concentration is increased, tree anodic shoulders (A, B and C) were observed (Fig. 1) for the respective potential values of 1.33, 1.47 and 1.78 V *vs.* Ag/AgCl. Additionally, the three anodic peaks A, B and C are diffusion controlled (inset of Fig. 1) as the peak current density (i_{peak}) is directly proportional to ATL concentration (Boye et al., 2006).

The comparison of the previous results with the cyclic voltammogram of the supporting electrolyte alone in solution (Fig. 1) corroborate that ATL can interact with this electrode, resulting in a direct electron transfer (direct oxidation). Furthermore, as the Nb/BDD_{2500} anode has a relative high content of carbon-sp^2 impurities (da Silva et al., 2018), higher adsorption sites on the electrode surface are available, favoring the direct ATL oxidation (peaks A, B, C) and SO_4^{2-} adsorption (shoulder I). Therefore, consequently, ATL can be oxidized by both mechanisms, direct and/or mediated oxidation, depending on the applied potential.

Fig. 1

3.2 Influence of the applied current density in ATL oxidation

In electrochemical processes, an increase in the applied current density can improve the oxidation rate, due to the higher amount of $^{\bullet}OH$ radicals generated and the discharge of the organic compounds on the electrode surface. Fig. 2 shows the effect of the applied current density on the degradation (Fig. 2a) and mineralization (Fig. 2b) of ATL. The degradation of ATL at the applied current densities of 5, 10 and 20 mA cm^{-2}

visually follows a linear decay typical of a pseudo zero-order kinetics, reaching degradation values of 50, 62 and 82% at the end of the electrolysis time, respectively. However, for the highest current density of 40 mA cm^{-2}, the degradation takes on a visual exponential character typical of a pseudo first-order kinetics, presenting an increase of the speed of the reaction until reaching the complete degradation of the ATL at 150 min. Finally, for the applied current density of 30 mA cm^{-2}, in the range of 0 – 75 min, the oxidation of ATL follows a linear relationship between the normalized ATL concentration and time, but for longer times, an exponential relationship is observed. Such a result can be motivated by a degradation pathway exchange and/or an exchange of the mechanisms that controls the AAO (Serrano et al., 2002; Sirés et al., 2010).

The mineralization data (Fig. 2b), presents a similar behavior to that observed in Fig. 2a. Comparing both figures, it is inferred that the degradation of the ATL is faster than its mineralization for all applied current densities. When applying low values of current densities (5, 10 and 20 mA cm^{-2}) the mineralization rates at the end of the assays were 36, 46 and 50%, respectively. For 30 and 40 mA cm^{-2}, a mineralization rate of approximately 75% was reached at 120 min of electrolysis and, after that time, no progress in the mineralization was observed. This fact can be explained by the low reactivity of the intermediate products generated, and also by the mass transport limitation of these species to the surface of the electrode due to their low concentration in the bulk solution. Similar results for ATL degradation and mineralization were obtained by Sirés et al. when they applied bulk electrolysis using a BBD anode and electro-Fenton processes (Sirés et al., 2010), and by Murugananthan et al. Using a BDD anode for the mineralization of ATL in different electrolytes (Murugananthan et al., 2011).

Moreover, ions chromatograms obtained in the treated solutions at the end of the electrolysis revealed the accumulation of NH_4^+ in all cases. Nitrate ions concentration was negligible in comparison to that of ammonium.

Fig. 2.

3.3 Effect of the Sodium Sulfate concentration on the Atenolol oxidation

In order to evaluate the influence of the supporting electrolyte on ATL degradation and mineralization, experiments with increasing amounts of Na_2SO_4 were performed. Fig. 3 and 4 present the same data as that presented in Fig. 2 with higher values of Na_2SO_4 concentration. Despite of the increase in Na_2SO_4 concentration, the degradation data presented in Fig. 2a and 3a show similar results. The main difference is observed at 30 and 40 mA cm^{-2}: in the case with the lowest concentration of sodium sulphate (0.014 M) the degradation was total at 150 min for both applied current values, whereas for 0.028 M Na_2SO_4 the total degradation is reached at higher times.

In terms of mineralization, again the results presented in Fig. 2b and 3b are quite similar for 5, 10 and 20 mA cm^{-2}. However, for 30 and 40 mA cm^{-2} the mineralization rate reached in the experiment at 0.028 M Na_2SO_4 was lower than that obtained at 0.014 M Na_2SO_4. One possible explanation for the lower degradation and mineralization obtained for the highest values of current density (30 and 40 mA cm^{-2}) and 0.028 M Na_2SO_4, is the higher availability of sulfate ions, that can compete with the $^{\bullet}OH$ radicals for the oxidation of the organic matter, especially at high current densities, depending on the experiments conditions, like pH (Wojnárovits and Takács, 2019).

The results corresponding to the highest value of Na_2SO_4 concentration tested (0.056 M) are presented in Fig. 4a and b for the degradation and mineralization of ATN, respectively. It is evident that the degradation is practically total, independently of the applied current density, after 180 min. The increase in Na_2SO_4 concentration increases the mineralization velocity; however, the global mineralization degree reached is similar to that previously observed with the lowest concentrations of sodium sulfate.

The ATN degradation may results in distinct transformation products besides CO_2, H_2O and inorganic ions (NH_4^+ - NO_3^-). The ATN mineralization (CO_2, H_2O and inorganic ions) was accomplished in the TOC analysis, however, the ATN transformation products can change according to applied current density, pH, oxidation mechanisms and involved ions/radicals ($SO_4^{\bullet-}$ - $S_2O_8^{2-}$ - $^{\bullet}OH$ (Miao et al., 2018; Rodriguez-Chueca et al., 2019; da Silva et al., 2019). The degradations processes can start by hydroxylation, deamination, ether bond fracture and dealkylation, mainly when sulfate oxidant species are involved (Miao et al., 2018). As reported in a previous work (da Silva et al., 2019), the ATN oxidation occurs at every applied current density under study and it is not affected strongly by the pH, resulting in direct oxidation and/or mediated by $SO_4^{\bullet-}$, $S_2O_8^{2-}$ and $^{\bullet}OH$. However, the operational parameters can affect the ATN degradation pathway, mainly the applied current density. At higher i, the total N is rapidly released from the ATN molecule and converted to NH_4^+. Nevertheless, for lower i, the total N was not completely oxidized, leading to organic nitrogenized byproducts (da Silva et al., 2019). Based on this information, a simplified degradation pathway was proposed (Fig. SM-1).

Fig. 3.

Fig. 4.

Some studies have demonstrated that the electrochemical degradation of organics follows a mixed (first and zero) order kinetics, depending on the initial compound concentration and applied current density (Rodgers and Bunce, 1999; Li et al., 2008; Chatzisymeon et al., 2009; Lin et al., 2013). In these studies, it was assumed that the main reaction was between ATL and hydroxyl radicals, and the rate equation depends on both the concentration of ATL and the concentration of $^{\bullet}OH$ radicals. However, for a given applied current density, the concentration of $^{\bullet}OH$ radicals can be considered constant, and the rate equation can be considered as pseudo-first order, and can be characterized by pseudo-first order reaction rate constant, k_{1st}.

As can be seen in Fig. 2, the experimental data can be well fitted to a pseudo-first order reaction for high applied current densities, where the amount of $^{\bullet}OH$ radicals is very high and the overall reaction is limited by the transport of ATL from the bulk solution to the proximities of the electrode where it reacts with $^{\bullet}OH$ radicals. For low applied current densities, the rate of $^{\bullet}OH$ radicals generation at the anode is slower than the rate of arrival of ATL molecules. In this case, the reaction is pseudo-zero order, and can be characterized by pseudo-zero order reaction rate constant, k_{zero}.

As can be seen in Fig. 2a, 3a and 4a, for low applied current densities and low electrolysis times (high ATL concentration in the bulk solution), pseudo-zero order kinetics is observed, while for high applied current densities, or high electrolysis times (low ATL concentration in the bulk solution), the process is mass transport controlled, and a pseudo-first order kinetics is observed. Table SM-1 summarizes the estimated

values of k_{zero} and k_{1st} based on the assumption of pseudo-zero or pseudo-first order kinetics, depending on the applied current density or the electrolysis time, while Fig. 5 shows the effect of the applied current density on k_{zero} (Fig 5a) and k_{1st} (Fig. 5b) for the different concentrations of supporting electrolyte under study.

As can be seen in Fig. 5a, for the lowest concentrations of sulfate ions of 0.014 and 0.028 M, similar values of k_{zero} are obtained, while the k_{zero} values increase considerably for the highest sulfate concentration. For the three sulfate concentrations, k_{zero} increases proportionally to the applied current density, suggesting that a constant $^{\bullet}OH$ concentration reacts with ATL in the bulk, and that higher constant concentrations of $^{\bullet}OH$ are formed with the applied current density. However, as can be seen in Fig. 5b, when the process is mass transport controlled, for high applied current densities and high electrolysis times, there is an excess of $^{\bullet}OH$ radicals, and the rate constant k_{1st} did not increase proportionally with the applied current density, which confirms the progressive enhancement of parasitic reactions.

On the other hand, higher values of k_{zero} and k_{1st} are obtained for the highest concentration of sulfate ions of 0.056 M. Some studies have reported the efficiency of the $SO_4^{\bullet-}$ and $S_2O_8^{2-}$ on the contaminant degradation, due to some advantages over the $^{\bullet}OH$ radical, such as similar redox potential to $^{\bullet}OH$ (E^0 ($SO_4^{\bullet-}$/ SO_4^{2-}) = 2.5 – 3.1 V) and a wide range of working pH (2 - 8) (Liang and Su, 2009; Matta et al., 2011; Lee et al., 2015). In addition, $SO_4^{\bullet-}$ has longer half-life (30 - 40 µs) than $^{\bullet}OH$ (< 1 µs) because $SO_4^{\bullet-}$ tend to react through electron transfer reactions while $^{\bullet}OH$ tend to react by unsaturated bonds and H-abstraction, besides being able to react in the bulk solution (Rastogi et al.,

2009). Moreover, the $SO_4^{\bullet-}$ radicals are more selective than $^{\bullet}OH$ ones (Wojnárovits and Takács, 2019).

Although, different studies prove that sulfate reactive species play an important role in degradation, however do not lead to the complete mineralization of the compound (Song et al., 2018; Yang et al., 2018; Aimer et al., 2019). Another possible explanation for the incomplete mineralization of ATL could be related to the hydrodynamics of the reactor or the low concentration and/or reactivity of the degradation products, such as the carboxylic acids (Hamza et al., 2009; Guinea et al., 2010).

Fig. 5.

3.4 Mineralization current efficiency

The effect of the supporting electrolyte concentration and the applied current density on the mineralization current efficiency (MCE) is presented in Fig. SM-2 on supplementary material. Low values of the MCE were obtained, reaching a maximum between 60 and 90 minutes of electrolysis. This maximum suggests the initial oxidation of the easily oxidizable byproducts of ATL, and the subsequent destruction of other byproducts more difficult to oxidize by the $^{\bullet}OH$ radicals. The time averaged values of the MCE presented in Fig. SM-2 as a function of the applied current density for the different concentrations of sulfate ions are presented in Fig. 6. For the lowest concentration of Na_2SO_4, the average values of this parameter were 8.4, 7.5, 4.4, 6.3, 5.0% for the respective values of current density of 5, 10, 20, 30 and 40 mA cm^{-2}. Although these results are quite similar, the lowest applied current of 5 mA cm^{-2} is presented as the more efficient in terms of ATL mineralization. The intermediate Na_2SO_4 concentration resulted in MCE average values of 14.7, 7.4, 4.3, 4.3, 3.5% for the respective 5, 10, 20,

30 and 40 mA cm^{-2}. As occurred previously the lowest value of current density shows the best results in terms of MCE. For the highest Na_2SO_4 concentration under study, the average values of MCE were 23.3, 12.7, 7.6, 6.5, 5.5% for 5, 10, 20, 30 and 40 mA cm^{-2}, respectively. Again, in this case, the increase in MCE takes place for the lowest values of current density (5 and 10 mA cm^{-2}). These low values of current efficiency are similar to those found by Sirés et al. when they applied an electro-Fenton process to ATL degradation (Sirés et al., 2010).

As can be seen in Fig. 6, MCE increases with the decrease of current density and the increase of sulfate concentration. Although higher values of applied current lead to increasing amount of hydroxyl radicals formed, these species are also more rapidly transformed into O_2, reaction (8), dimerization through reaction (9), or decomposition by H_2O_2, reaction (10) under very anodic conditions, which are not so effective in the ATL mineralization process (Hamza et al., 2009; Mora-Gomez et al., 2018). On the other hand, the increase of the MCE with the initial concentration of sulfate ions may be due to the more efficient production and activation of precursors, such as persulfate, which is more efficiently produced at high concentrations of sulfate ions (Serrano et al., 2002).

$$\mathrm{M}(^{\bullet}\mathrm{OH}) \rightarrow \mathrm{M} + \frac{1}{2}\mathrm{O_2} + \mathrm{H^+} + \mathrm{e^-} \tag{8}$$

$$2\mathrm{M}(^{\bullet}\mathrm{OH}) \rightarrow 2\mathrm{M} + \mathrm{H_2O_2} \tag{9}$$

$$\mathrm{H_2O_2} + \mathrm{M}(^{\bullet}\mathrm{OH}) \rightarrow \mathrm{M}(\mathrm{HO_2^{\bullet}}) + \mathrm{H_2O} \tag{10}$$

Fig. 6.

3.5 pH behavior

The pH is an important parameter in the advanced anodic oxidation (AAO) processes. Fig. 7 presents the pH of the treated solution as a function of the applied current and for every Na_2SO_4 solution concentration under study. With the exception of the highest applied current (40 mA cm^{-2}) and supporting electrolyte concentration (0.056 M Na_2SO_4), the pH decreases from its initial value (around 9). This pH variation may be due to the byproducts generation or stabilization reaction of reactive active electrogenerated species (Vasilie et al., 2018).

According to Hadj et al. (Hadj et al., 2017), AAO at BDD anodes works better at both acid and natural pH. Moreover, the redox potential of hydroxyl radicals is lower in alkaline conditions (E^0 ($^{\bullet}OH/H_2O$) = 1.8 V) than in acidic ones (E^0 ($^{\bullet}OH/H_2O$) = 2.8 V) (Rabaaoui and Allagui, 2012; Haidar et al., 2013). At pH ranges from 9 to 10 both radicals $^{\bullet}OH$ and $SO_4^{\bullet-}$ can coexist, although the $SO_4^{\bullet-}$ redox potential can be higher than $^{\bullet}OH$ in such a condition (Fang et al., 2012). Besides that, in alkaline pH, the $SO_4^{\bullet-}$ can also generate hydroxyl radical (Liang and Su, 2009). Such a finding could explain the increase in the mineralization velocity observed previously at 0.056 M Na_2SO_4 and 40 mA cm^{-2}.

Fig. 7.

4 Conclusions

The electrochemical characterization of the Nb/BDD anode employed for the ATN degradation showed that presents a high quality, low background current and high potential for OER. In addition, the ATL can be effectively oxidized directly and/or indirectly by the electrogenerated oxidants, such as hydroxyl radicals, persulfate ions and sulfate radicals.

The increase in applied current density represents a positive effect in the degradation and mineralization of the ATL, although the mineralization rate is always lower than the degradation one due to the generated intermediate products more difficult to destroy. ATN degradation and mineralization follow a mixed (first and zero) order kinetics depending on the applied current density. At high values of current density, the overall reaction is limited by the transport of ATL (pseudo first-order kinetics) whereas for low applied current densities, the rate of $^{\bullet}OH$ radicals generation at the anode is slower than the rate of arrival of ATL molecules (pseudo-zero order kinetics).

Sodium sulfate concentration also affects the degradation and mineralization of ATL. Estimated values of the reaction rate constants (k_{zero} and k_{1st}) based on the assumption of pseudo-zero or pseudo-first order kinetics were calculated, indicating that both parameters increased with Na_2SO_4 concentration due the higher production of sulfate reactive species, such as radicals ($SO_4^{\bullet -}$) and ions ($S_2O_8^{2-}$), that play an important role in degradation.

MCE increases with the decrease of current density, due to the lower amount of $^{\bullet}OH$ present in solution since this species could be rapidly wasted in parasitic reactions;

and the increase of sulfate concentration, due to the more efficient production of persulfate.

Acknowledgments

The authors thank the financial support from the Ministerio de Economía y Competitividad (Spain) under projects CTQ2015-65202-C2-1-R and RTI2018-101341-B-C21, co-financed with FEDER funds. The authors thank to FAPERGS, CAPES, FINEP and CNPQ.

References

Abdessamad, N., Akrout, H., Hamdaoui, G., Elghniji, K., Ksibi, M., 2013. Evaluation of the efficiency of monopolar and bipolar BDD electrodes for electrochemical oxidation of anthraquinone textile synthetic effluent for reuse. Chemosphere 93, 1309–1316.

Aimer, Y., Benali, O., Groenen Serrano, K., 2019. Study of the degradation of an organophosphorus pesticide using electrogenerated hydroxyl radicals or heat-activated persulfate. Sep. Purif. Technol. 208, 27–33.

Atinkpahoun, C.N.H., Dinh, N., Pontvianne, S., Poirot, H., Leclerc, J., Pons, M., Soclo, H.H., 2018. Population mobility and urban wastewater dynamics. Sci. Total Environ. 623, 1431–1437.

Baken, K.A., Sjerps, R.M.A., Schriks, M., Wezel, A.P. Van, 2018. Toxicological risk assessment and prioritization of drinking water relevant contaminants of emerging concern. Environ. Int. J. 118, 293–303.

Barreto, J.P. de P., Araújo, K.C. de F., de Araújo, D.M., Martínez-Huitle, C.A., 2015. Effect of sp^3/sp^2 ratio on boron doped diamond films for producing persulfate. ECS Electrochem. Lett. 4, E9–E11.

Belenguer, V., Martinez-Capel, F., Masiá, A., Picó, Y., 2014. Patterns of presence and concentration of pesticides in fish and waters of the júcar river (eastern spain). J. Hazard. Mater. 265, 271–279.

Benson, R., Conerly, O.D., Sander, W., Batt, A.L., Boone, J.S., Furlong, E.T., Glassmeyer, S.T., Kolpin, D.W., Mash, H.E., Schenck, K.M., Ellen, J., 2017. Human health screening and public health signi fi cance of contaminants of emerging concern detected in public water supplies. Sci. Total Environ. 579, 1643–1648.

Boye, B., Brillas, E., Marselli, B., Michaud, P.A., Comninellis, C., Farnia, G., Sandonà, G., 2006. Electrochemical incineration of chloromethylphenoxy herbicides in acid medium by anodic oxidation with boron-doped diamond electrode. Electrochim. Acta 51, 2872–2880.

Brillas, E., Sirés, I., Oturan, M.A., 2009. Electro-Fenton process and related electrochemical technologies based on Fenton's reaction chemistry. Chem. Rev. 109, 6570–6631.

Brocenschi, R.F., Rocha-filho, R.C., Bocchi, N., Biaggio, S.R., 2016. Electrochemical degradation of estrone using a boron-doped diamond anode in a fi lter-press reactor. Electrochim. Acta 197, 186–193.

Chatzisymeon, E., Dimou, A., Mantzavinos, D., Katsaounis, A., 2009. Electrochemical oxidation of model compounds and olive mill wastewater over DSA electrodes : 1. The case of Ti/IrO_2 anode. J. Hazard. Mater. 167, 268–274.

Chianca, D., Moura, D., Kérzia, C., Araújo, C. De, Zanta, C.L.P.S., Salazar, R., Martínez-huitle, C.A., 2014. Active chlorine species electrogenerated on Ti/$Ru_{0.3}Ti_{0.7}O_2$ surface: Electrochemical behavior, concentration determination and their application. J. Electroanal. Chem. 731, 145–152.

Ciríaco, L., Anjo, C., Correia, J., Pacheco, M.J., Lopes, A., 2009. Electrochemical degradation of Ibuprofen on Ti/Pt/PbO_2 and Si/BDD electrodes. Electrochim. Acta 54, 1464–1472.

Clematis, D., Cerisola, G., Panizza, M., 2017. Electrochemical oxidation of a synthetic dye using a BDD anode with a solid polymer electrolyte. Electrochem. Commun. 75, 21–24.

da Silva, S.W., Navarro, E.M.O., Rodrigues, M.A.S., Bernardes, A.M., Pérez-Herranz, V., 2018. The role of the anode material and water matrix in the electrochemical

oxidation of norfloxacin. Chemosphere 210, 615–623.

da Silva, S.W., do Prado, J.M., Heberle, A.N.A., Schneider, D.E., Rodrigues, M.A.S., Bernardes, A.M., 2019. Electrochemical advanced oxidation of Atenolol at Nb/BDD thin film anode, J. Electroanal. Chem. 844, 27–33.

Davis, J., Baygents, J.C., Farrell, J., 2014. Understanding persulfate production at boron doped diamond film anodes. Electrochim. Acta 150, 68–74.

de Wit, C.A., Balmer, J., Muir, D.C.G., Vorkamp, K., Wilson, S., 2019. Chemicals of emerging arctic concern: Preface. Emerg. Contam. 5, 1–3.

Dominguez, C.M., Oturan, N., Romero, A., Santos, A., Oturan, M.A., 2018. Lindane degradation by electrooxidation process : Effect of electrode materials on oxidation and mineralization kinetics. Water Res. 135, 220–230.

Einaga, Y., Foord, J.S., Swain, G.M., 2014. Diamond electrodes: Diversity and maturity. MRS Bull. 39, 525–532.

Espinoza, L.C., Henríquez, A., Contreras, D., Salazar, R., 2018. Evidence for the production of hydroxyl radicals at boron-doped diamondelectrodes with different sp^3/sp^2 ratios and its relationship with the anodicoxidation of aniline. Electrochem. commun. 90, 3–6.

Fang, G.D., Dionysiou, D.D., Wang, Y., Al-Abed, S.R., Zhou, D.M., 2012. Sulfate radical-based degradation of polychlorinated biphenyls: Effects of chloride ion and reaction kinetics. J. Hazard. Mater. 227–228, 394–401.

Frishman, W.H., 2016. Beta-adrenergic receptor blockers in hypertension: Alive and Well. Prog. Cardiovasc. Dis. 59, 247–252.

Garcia-Segura, S., Vieira dos Santos, E., Martínez-Huitle, C.A., 2015. Role of sp^3/sp^2 ratio on the electrocatalytic properties of boron-doped diamond electrodes: A mini review. Electrochem. commun. 59, 52–55.

Godoy, A.A., Kummrow, F., Pamplin, P.A.Z., 2015. Occurrence, ecotoxicological effects and risk assessment of antihypertensive pharmaceutical residues in the aquatic environment - A review. Chemosphere 138, 281–291.

Guinea, E., Garrido, J.A., Rodríguez, R.M., Cabot, P.-L., Arias, C., Centellas, F., Brillas, E., 2010. Degradation of the fluoroquinolone enrofloxacin by electrochemical advanced oxidation processes based on hydrogen peroxide electrogeneration. Electrochim. Acta 55, 2101–2115.

García-Montoya, M.F., Gutiérrez-Granados,S., Alatorre-Ordaz, A., Galindo, R., Ornelas, R., Peralta-Hernández, J.M., 2015. Application of electrochemical / BDD process for the treatment wastewater effluents containing pharmaceutical compounds. J. Ind. Eng. Chem. 31, 238–243.

Hadj, A., Angelo, A.D., Ammar, S., Gadri, A., Galia, A., Scialdone, O., 2017. Electrochemical treatment of aqueous solutions of catechol by various electrochemical advanced oxidation processes : Effect of the process and of operating parameters. J. Electroanal. Chem. 796, 1–8.

Haidar, M., Dirany, A., Sirés, I., Oturan, N., Oturan, M.A., 2013. Electrochemical degradation of the antibiotic sulfachloropyridazine by hydroxyl radicals generated at a BDD anode. Chemosphere 91, 1304–1309.

Hamza, M., Abdelhedi, R., Brillas, E., Sirés, I., 2009. Comparative electrochemical degradation of the triphenylmethane dye Methyl Violet with boron-doped diamond and Pt anodes. J. Electroanal. Chem. 627, 41–50.

He, Y., Lin, H., Guo, Z., Zhang, W., Li, H., Huang, W., 2019. Recent developments and advances in boron-doped diamond electrodes for electrochemical oxidation of organic pollutants. Sep. Purif. Technol. 212, 802–821.

Isarain-Chávez, E., Rodríguez, R.M., Cabot, P.L., Centellas, F., Arias, C., Garrido, J.A.,

Brillas, E., 2011. Degradation of pharmaceutical beta-blockers by electrochemical advanced oxidation processes using a flow plant with a solar compound parabolic collector. Water Res. 45, 4119–4130.

Kanakaraju, D., Glass, B.D., Oelgemöller, M., 2018. Advanced oxidation process-mediated removal of pharmaceuticals from water: A review. J. Environ. Manage. 219, 189–207.

Kaur, R., Kushwaha, J.P., Singh, N., 2019. Amoxicillin electro-catalytic oxidation using Ti/RuO_2 anode : Mechanism , oxidation products and degradation pathway. Electrochim. Acta 296, 856–866.

Lee, H., Lee, H.J., Jeong, J., Lee, J., Park, N.B., Lee, C., 2015. Activation of persulfates by carbon nanotubes: Oxidation of organic compounds by nonradical mechanism. Chem. Eng. J. 266, 28–33.

Li, S., Bejan, D., McDowell, M.S., Bunce, N.J., 2008. Mixed first and zero order kinetics in the electrooxidation of sulfamethoxazole at a boron-doped diamond (BDD) anode. J. Appl. Electrochem. 151–159.

Liang, C., Su, H.W., 2009. Identification of sulfate and hydroxyl radicals in thermally activated persulfate. Ind. Eng. Chem. Res. 48, 5558–5562.

Lin, H., Niu, J., Xu, J., Li, Y., Pan, Y., 2013. Electrochemical mineralization of sulfamethoxazole by Ti/SnO_2-Sb/Ce-PbO_2 anode : Kinetics, reaction pathways, and energy cost evolution. Electrochim. Acta 97, 167–174.

Luo, Y., Guo, W., Ngo, H.H., Nghiem, L.D., Hai, F.I., Zhang, J., Liang, S., Wang, X.C., 2014. A review on the occurrence of micropollutants in the aquatic environment and their fate and removal during wastewater treatment. Sci. Total Environ. 473–474, 619–641.

Matta, R., Tlili, S., Chiron, S., Barbati, S., 2011. Removal of carbamazepine from urban

wastewater by sulfate radical oxidation. Environ. Chem. Lett. 9, 347–353.

Miao, D., Peng, J., Zhou, X., Qian, L., Wang, M., Zhai, L., Gao, S., 2018. Oxidative degradation of atenolol by heat-activated persulfate: Kinetics, degradation pathways and distribution of transformation intermediates. Chemosphere. 207, 174–182.

Ministério da Saúde, 2012. Manual de Orientações àsFarmácias e Drogarias Credenciadas No “Aqui Tem Farmácia Popular .”

Mora-Gomez, J., Ortega, E., Mestre, S., Pérez-Herranz, V., García-Gabaldón, M., 2019. Electrochemical degradation of norfloxacin using BDD and new Sb-doped SnO_2 ceramic anodes in an electrochemical reactor in the presence and absence of a cation-exchange membrane. Sep. Purif. Technol. 208, 68–75.

Murugananthan, M., Latha, S.S., Raju, G.B., Yoshihara, S., 2011. Role of electrolyte on anodic mineralization of atenolol at boron doped diamond and Pt electrodes. Sep. Purif. Technol. 79, 56–62.

Pacheco, M.J., Santos, V., Ciríaco, L., Lopes, A., 2011. Electrochemical degradation of aromatic amines on BDD electrodes. J. Hazard. Mater. 186, 1033–1041.

Panizza, M., Cerisola, G., 2009. Direct and mediated anodic oxidation of organic pollutants. Chem. Rev. 109, 6541–6569.

Panizza, M., Cerisola, G., 2005. Application of diamond electrodes to electrochemical processes. Electrochim. Acta 51, 191–199.

Periyasamy, S., Muthuchamy, M., 2018. Electrochemical oxidation of paracetamol in water by graphite anode : E ff ect of pH , electrolyte concentration and current density. J. Environ. Chem. Eng. 6, 7358–7367.

Polcaro, A.M., Mascia, M., Palmas, S., Vacca, A., 2004. Electrochemical degradation of diuron and dichloroaniline at BDD electrode. Electrochim. Acta 49, 649–656.

Provent, C., Haenni, W., Santoli, E., Rychen, P., 2004. Boron-doped diamond electrodes and microelectrode-arrays for the measurement of sulfate and peroxodisulfate. Electrochim. Acta 49, 3737–3744.

Rabaaoui, N., Allagui, M.S., 2012. Anodic oxidation of salicylic acid on BDD electrode: variable effects and mechanisms of degradation. J. Hazard. Mater. 243, 187–92.

Radjenovic, J., Petrovic, M., 2017. Removal of sulfamethoxazole by electrochemically activated sulfate: Implications of chloride addition. J. Hazard. Mater. 333, 242–249.

Rastogi, A., Al-Abed, S.R., Dionysiou, D.D., 2009. Sulfate radical-based ferrous-peroxymonosulfate oxidative system for PCBs degradation in aqueous and sediment systems. Appl. Catal. B: Environ. 85, 171–179.

Rodgers, J.D., Bunce, N.J., 1999. Electrochemical oxidation of chlorinated phenols. Environ. Sci. Technol. 1453–1457.

Rodríguez-Chueca, J., Garcia-Cañibano, C., Sarro, M., Encinas, Á., Medana, C., Fabbri, D., Calza, P., Marugán, J., 2019. Evaluation of transformation products from chemical oxidation of micropollutants in wastewater by photoassisted generation of sulfate radicals, Chemosphere. 226, 509–519.

Serrano, K., Michaud, P.A., Comninellis, C., Savall, A., 2002. Electrochemical preparation of peroxodisulfuric acid using boron doped diamond thin film electrodes. Electrochim. Acta 48, 431–436.

Sirés, I., Oturan, N., Oturan, M.A., 2010. Electrochemical degradation of β-blockers . Studies on single and multicomponent synthetic aqueous solutions. Water Res. 44, 3109–3120.

Song, H., Yan, L., Jiang, J., Ma, J., Zhang, Z., Zhang, J., Liu, P., Yang, T., 2018. Electrochemical activation of persulfates at BDD anode: Radical or nonradical

oxidation? Water Res. 128, 393–401.

Sousa, J.C.G., Ribeiro, A.R., Barbosa, M.O., Pereira, M.F.R., Silva, A.M.T., 2018. A review on environmental monitoring of water organic pollutants identified by EU guidelines. J. Hazard. Mater. 344, 146–162.

Souza, F.L., Saéz, C., Lanza, M.R.V., Cañizares, P., Rodrigo, M.A., 2016. The effect of the sp^3/sp^2 carbon ratio on the electrochemical oxidation of 2,4-D with p-Si BDD anodes. Electrochim. Acta 187, 119–124.

Souza, R.B.A., Ruotolo, L.A.M., 2013. Electrochemical treatment of oil refinery effluent using boron-doped diamond anodes. J. Environ. Chem. Eng. 1, 544–551.

Vasilie, S., Manea, F., Baciu, A., Pop, A., 2018. Dual use of boron-doped diamond electrode in antibiotics-containing water treatment and process control. Process Saf. Environ. Prot. 117, 446–453.

Vieno, N.M., Härkki, H., Tuhkanen, T., Kronberg, L., 2007. Occurrence of pharmaceuticals in river water and their elimination in a pilot-scale drinking water treatment plant. Environ. Sci. Technol. 41, 5077–5084.

Watanabe, T., Shimizu, T.K., Tateyama, Y., Kim, Y., Kawai, M., Einaga, Y., 2010. Giant electric double-layer capacitance of heavily boron-doped diamond electrode. Diam. Relat. Mater. 19, 772–777.

Wojnárovits, L., Takács, E., 2019. Rate constants of sulfate radical anion reactions with organic molecules: A review. Chemosphere 220, 1014–1032.

Xu, S., Zheng, J., Wu, Z., Liu, M., Wang, Z., 2018. Degradation of p -chloroaniline using an electrochemical ceramic micro fi ltration membrane with built-in electrodes. Electrochim. Acta 292, 655–666.

Yang, S.Q., Cui, Y.H., Liu, Y.Y., Liu, Z.Q., Li, X.Y., 2018. Electrochemical generation of persulfate and its performance on 4-bromophenol treatment. Sep. Purif. Technol.

207, 461–469.

Zabik, N.L., Anwar, S., Ziu, I., Martic-milne, S., 2019. Electrochimica Acta Electrochemical reactivity of bulky-phenols with superoxide anion radical. Electrochim. Acta 296, 174–180.

LIST OF FIGURES.

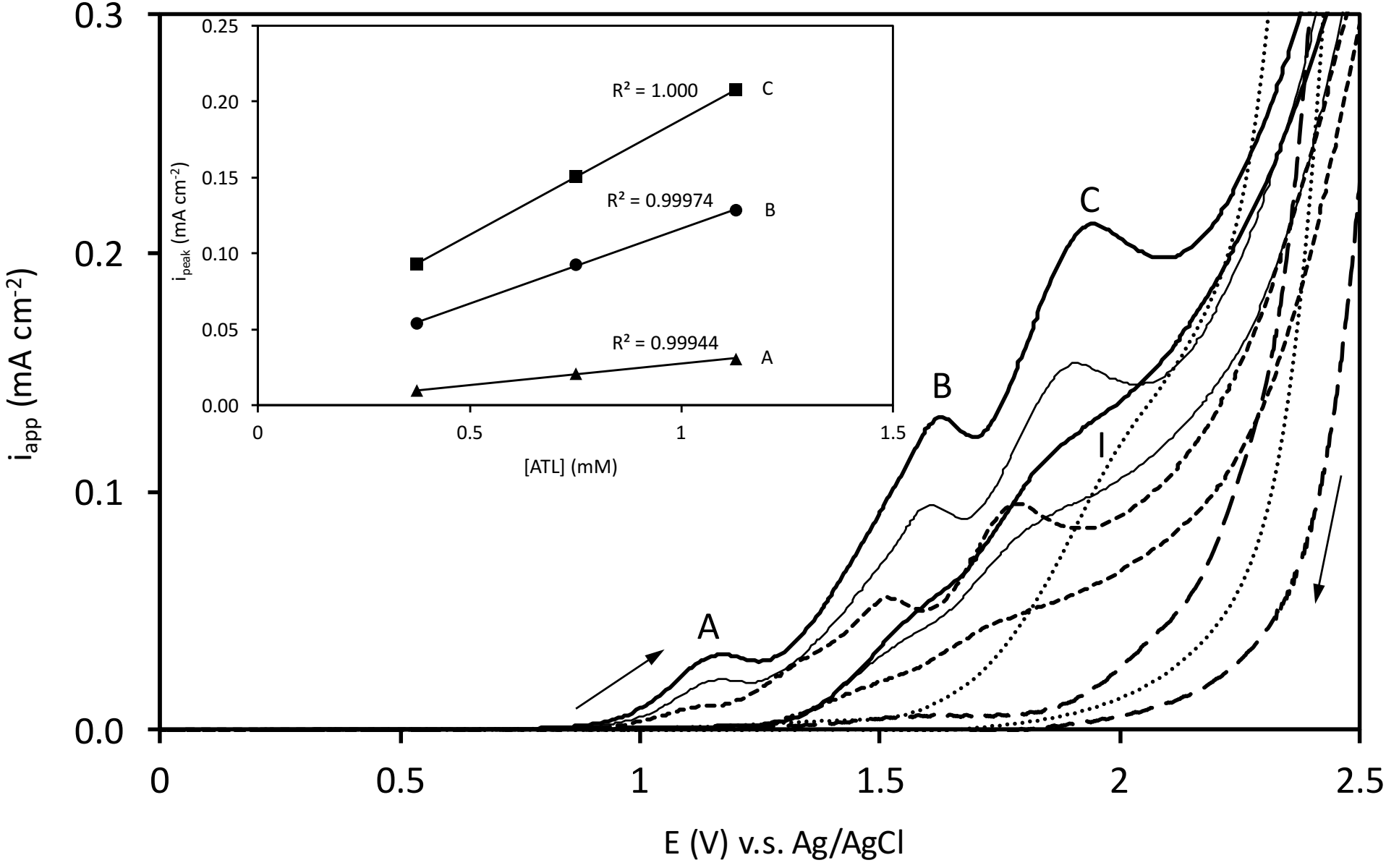
0.3
0.2
0.1
0.0
0
0.5
1
1.5
2
2.5
i_{app} (mA cm^{-2})
E (V) v.s. Ag/AgCl
A
B
C
I
0.25
0.20
0.15
0.10
0.05
0.00
0
0.5
1
1.5
i_{peak} (mA cm^{-2})
[ATL] (mM)
R^2 = 1.000
C
R^2 = 0.99974
B
R^2 = 0.99944
A

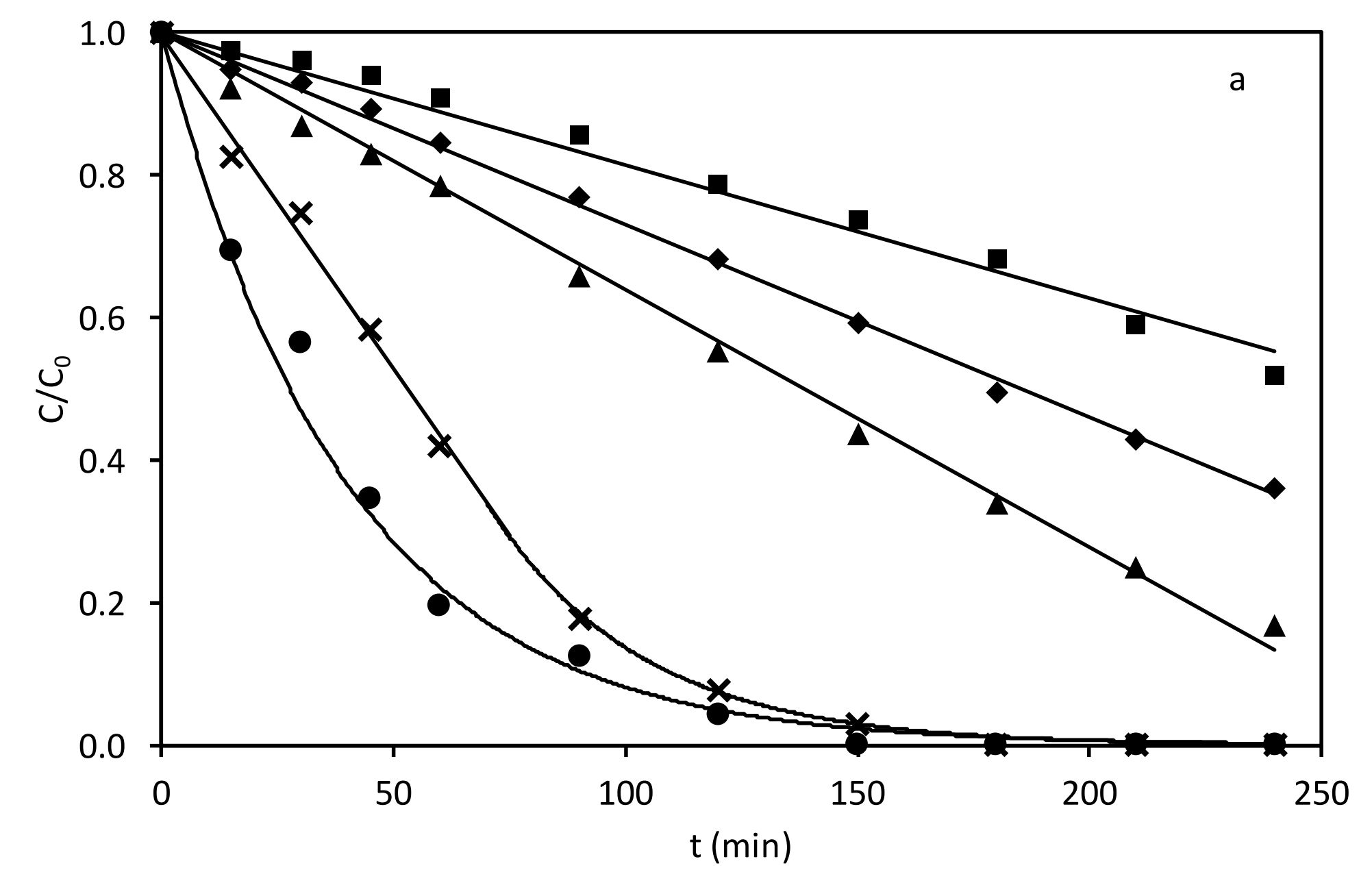
a
C/C0
t (min)
1.0
0.8
0.6
0.4
0.2
0.0
0
50
100
150
200
250

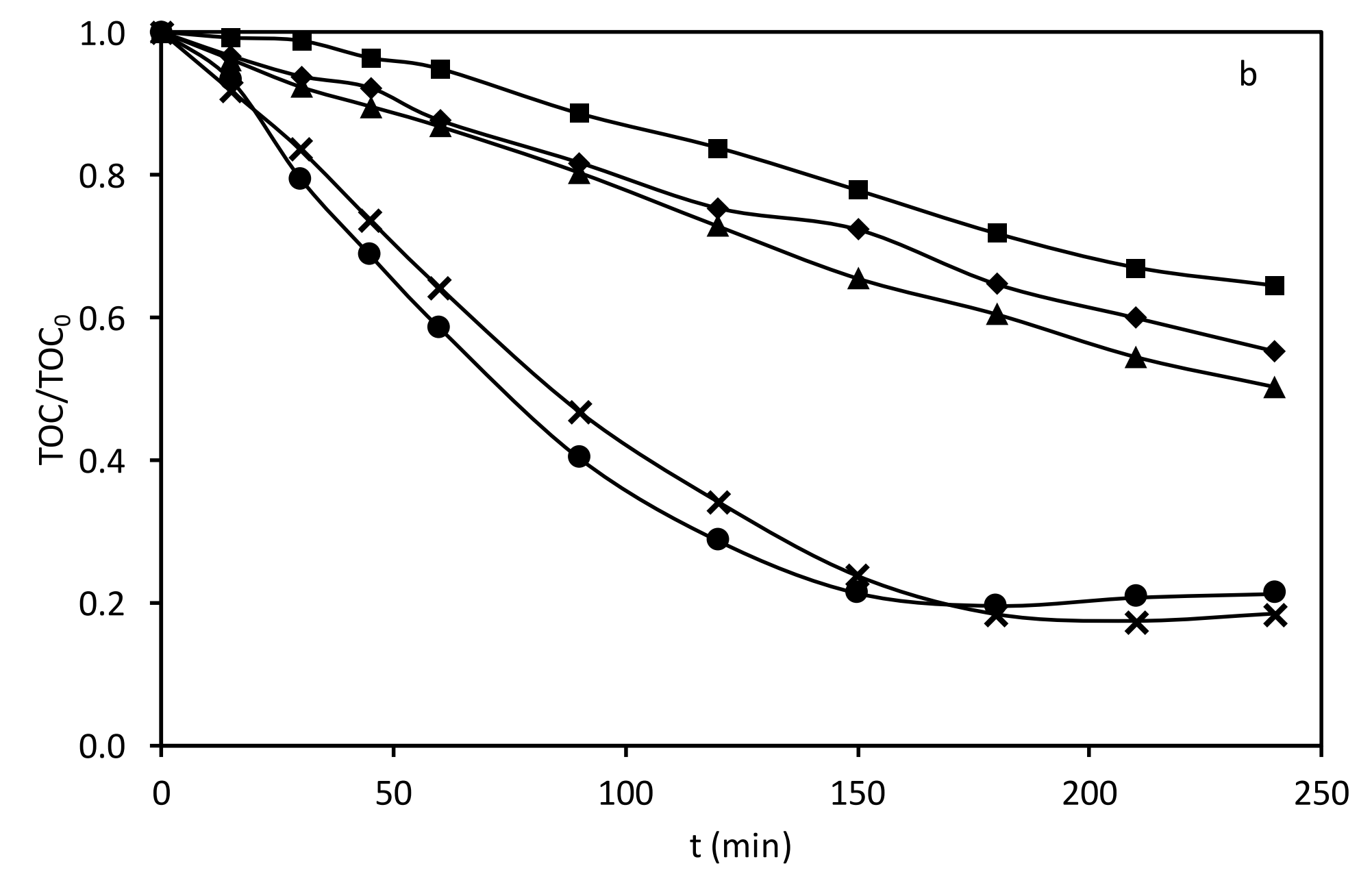
b
TOC/TOC0
t (min)
0.0
0.2
0.4
0.6
0.8
1.0
0
50
100
150
200
250

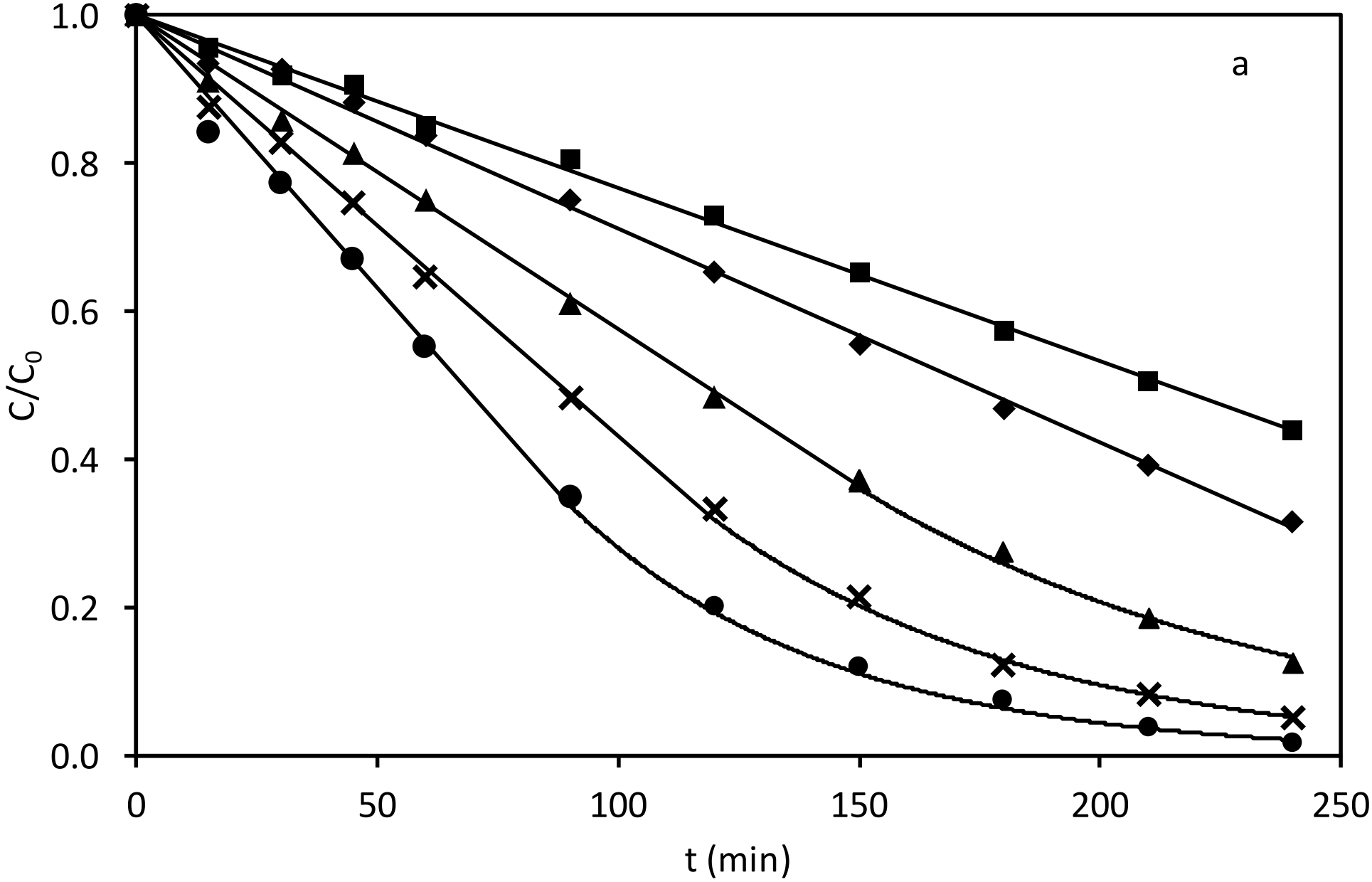
a
C/C0
t (min)
1.0
0.8
0.6
0.4
0.2
0.0
0
50
100
150
200
250

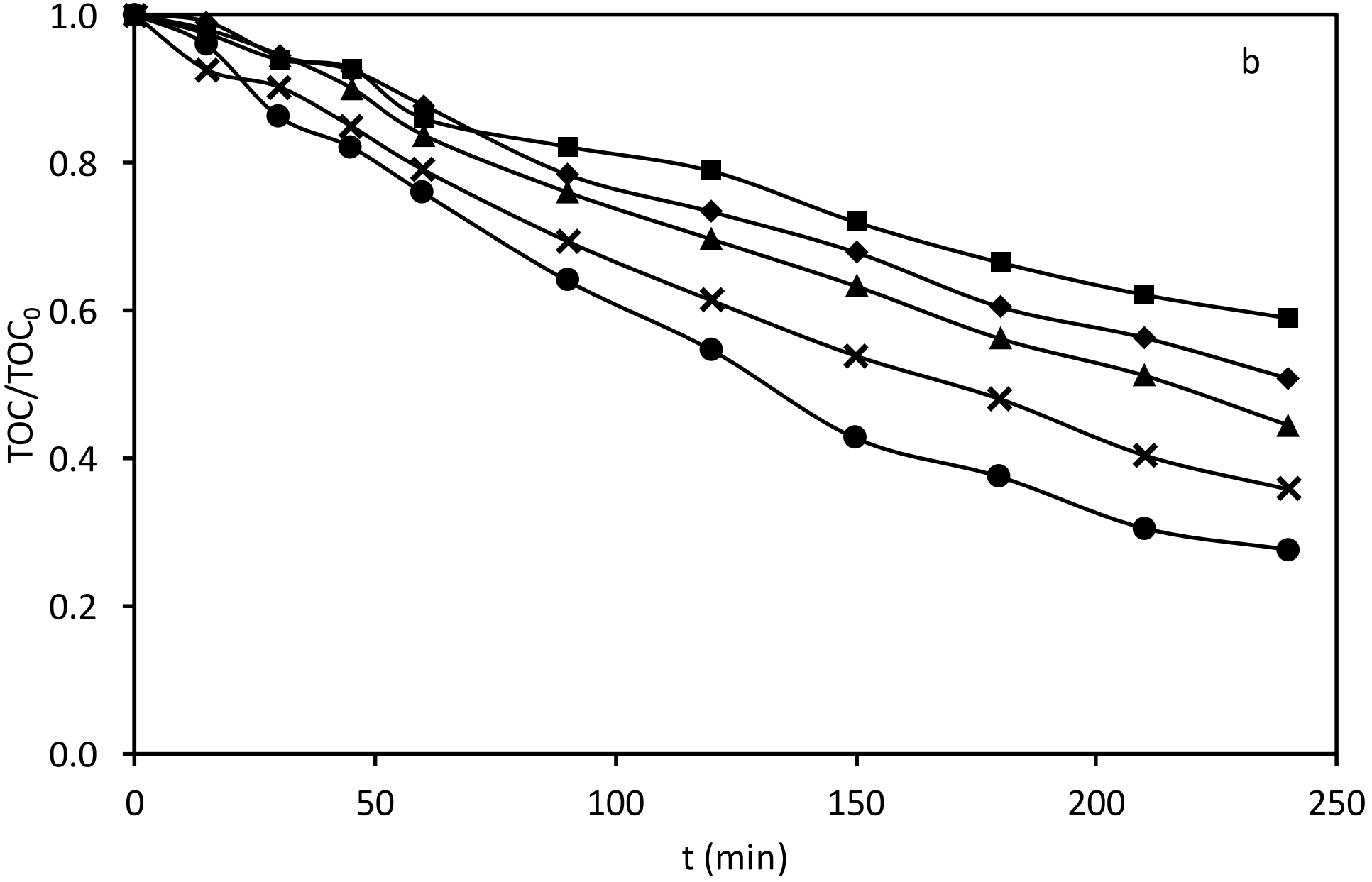
b
TOC/TOC0
1.0
0.8
0.6
0.4
0.2
0.0
0
50
100
150
200
250
t (min)

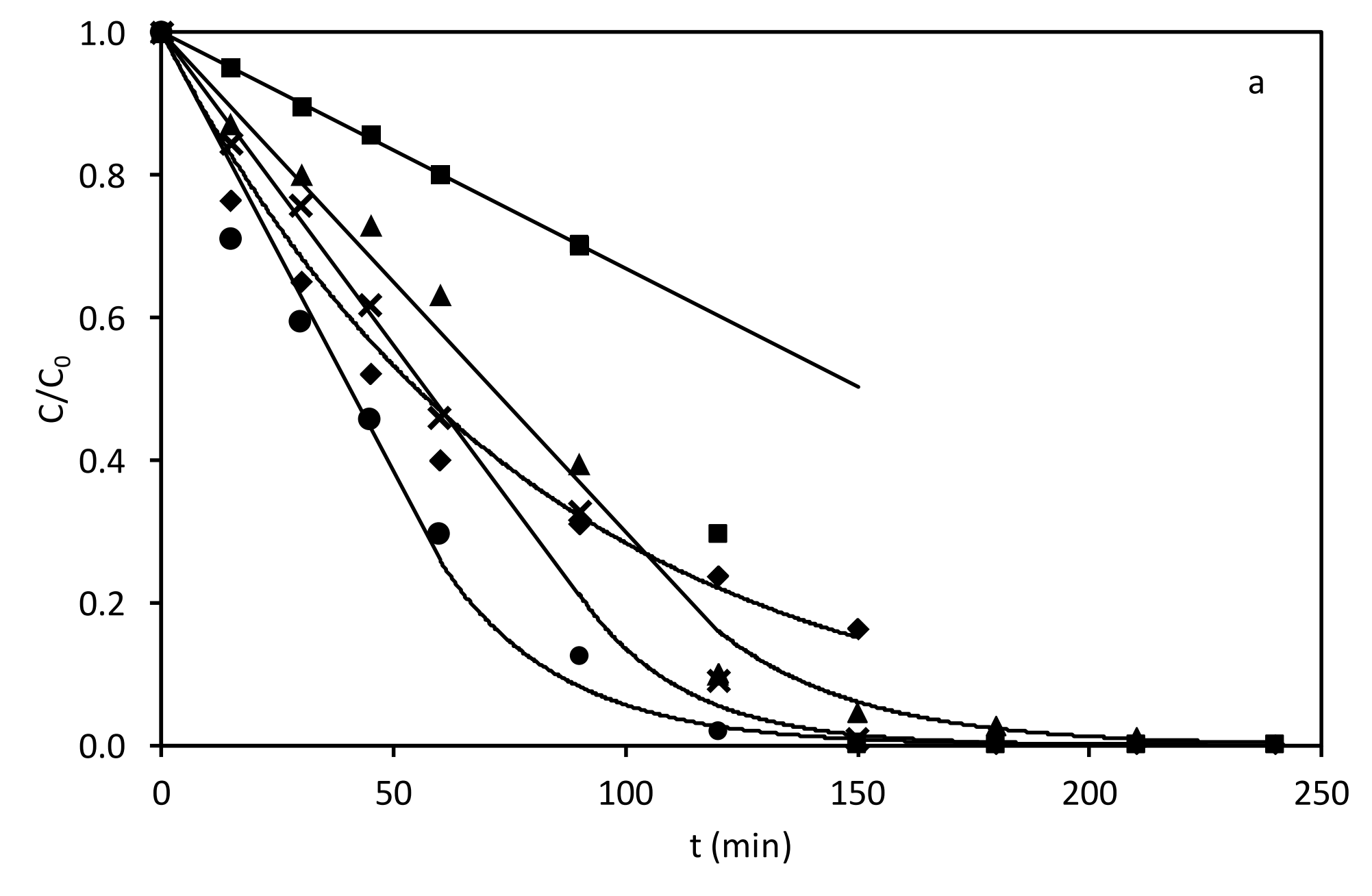
a
C/C0
t (min)
1.0
0.8
0.6
0.4
0.2
0.0
0
50
100
150
200
250

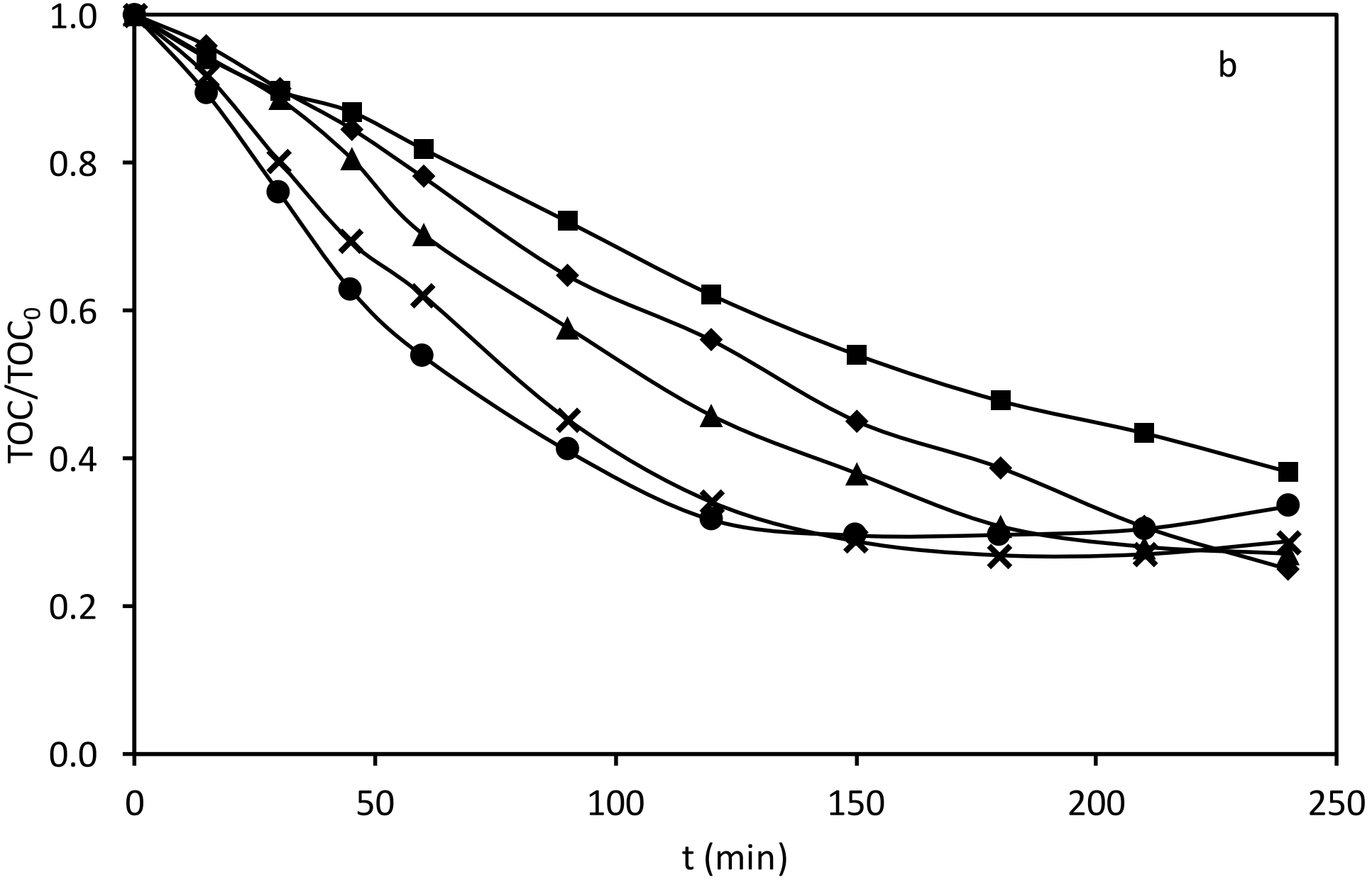
b
TOC/TOC0
t (min)
0.0
0.2
0.4
0.6
0.8
1.0
0
50
100
150
200
250

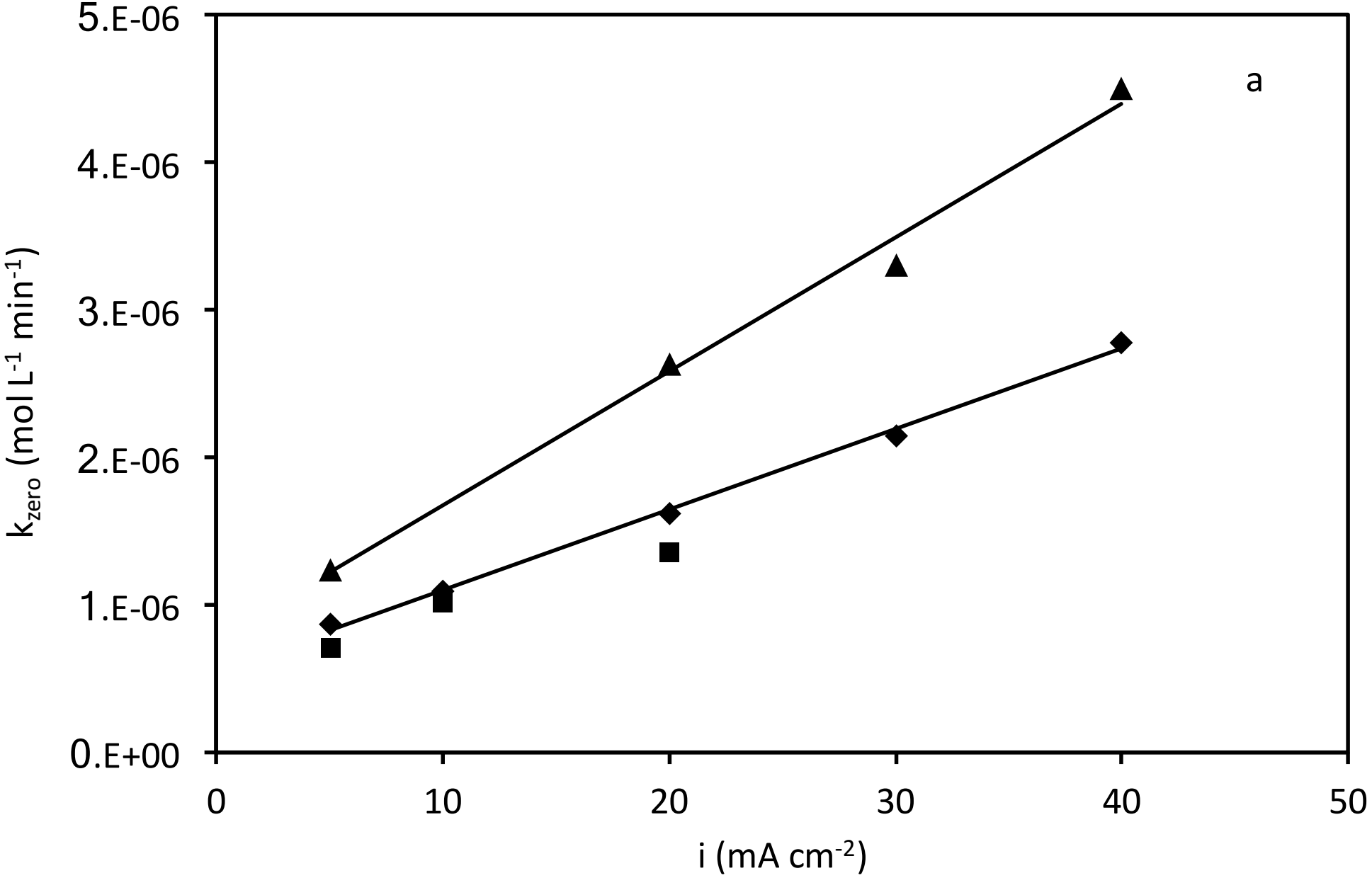
5.E-06
4.E-06
3.E-06
2.E-06
1.E-06
0.E+00
k_{zero} (mol L^{-1} min^{-1})
0
10
20
30
40
50
i (mA cm^{-2})
a

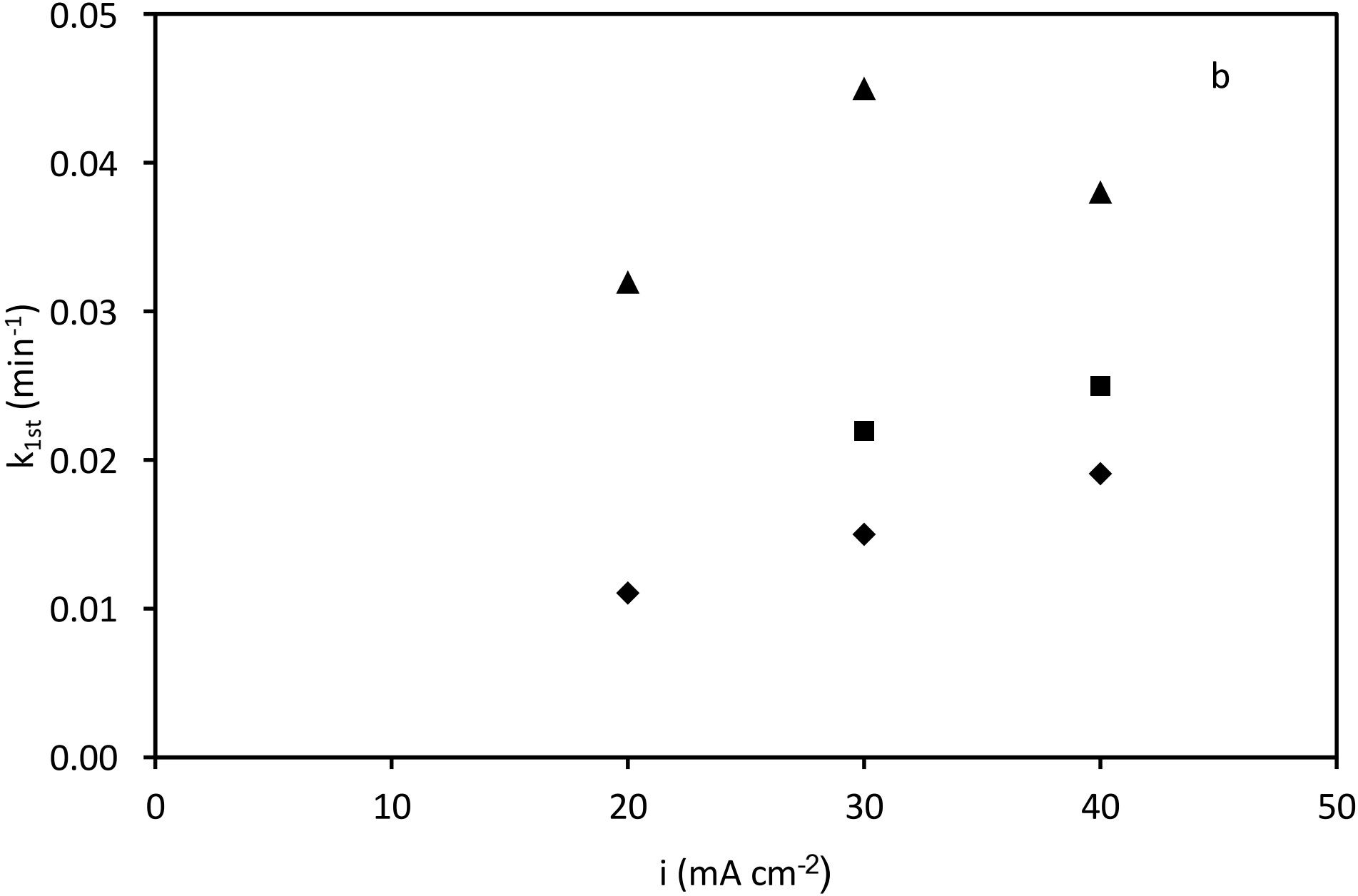
b
0.05
0.04
0.03
0.02
0.01
0.00
k_{1st} (min^{-1})
0
10
20
30
40
50
i (mA cm^{-2})

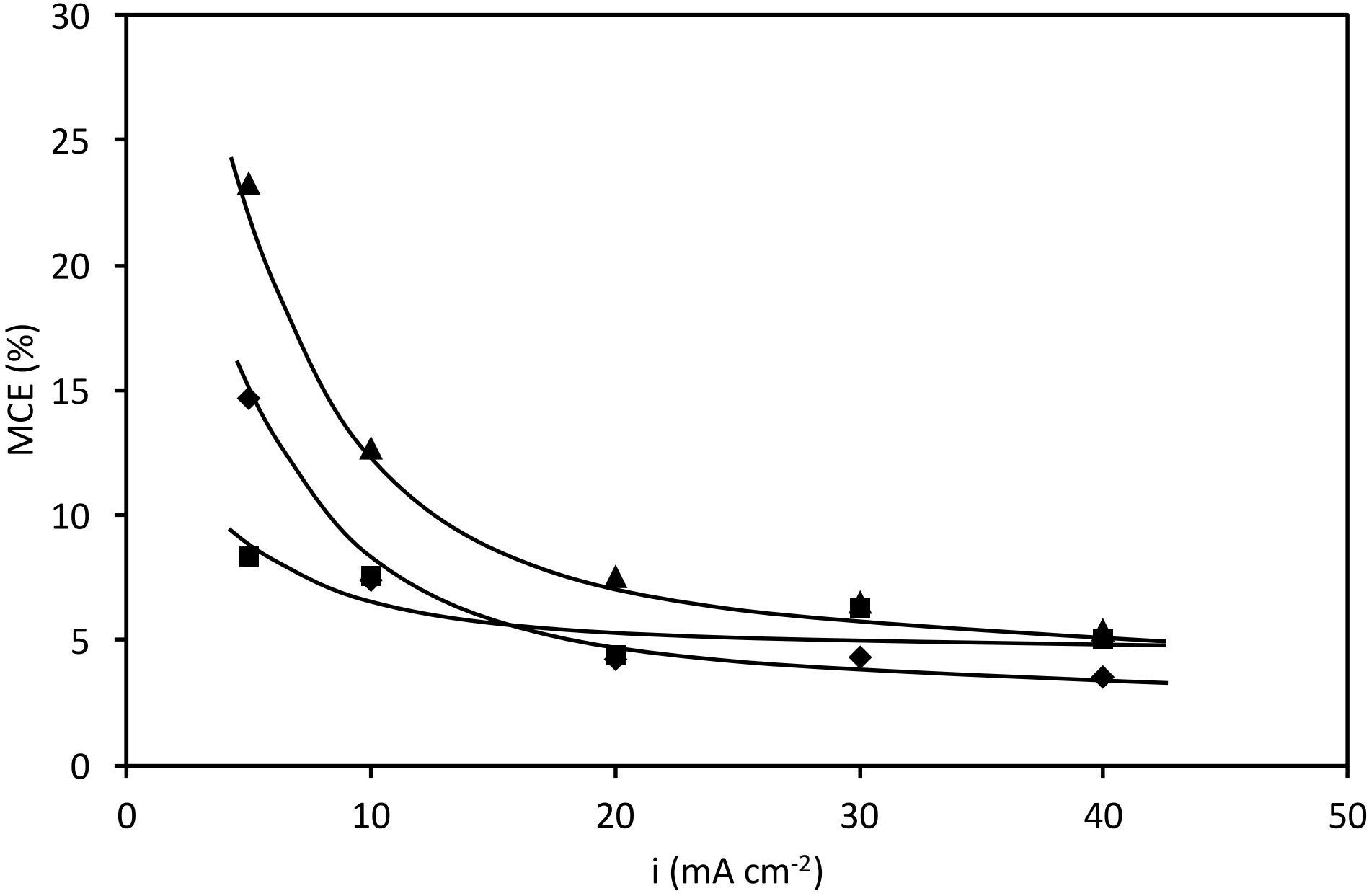
30
25
20
15
10
5
0
MCE (%)
0
10
20
30
40
50
i (mA cm-2)

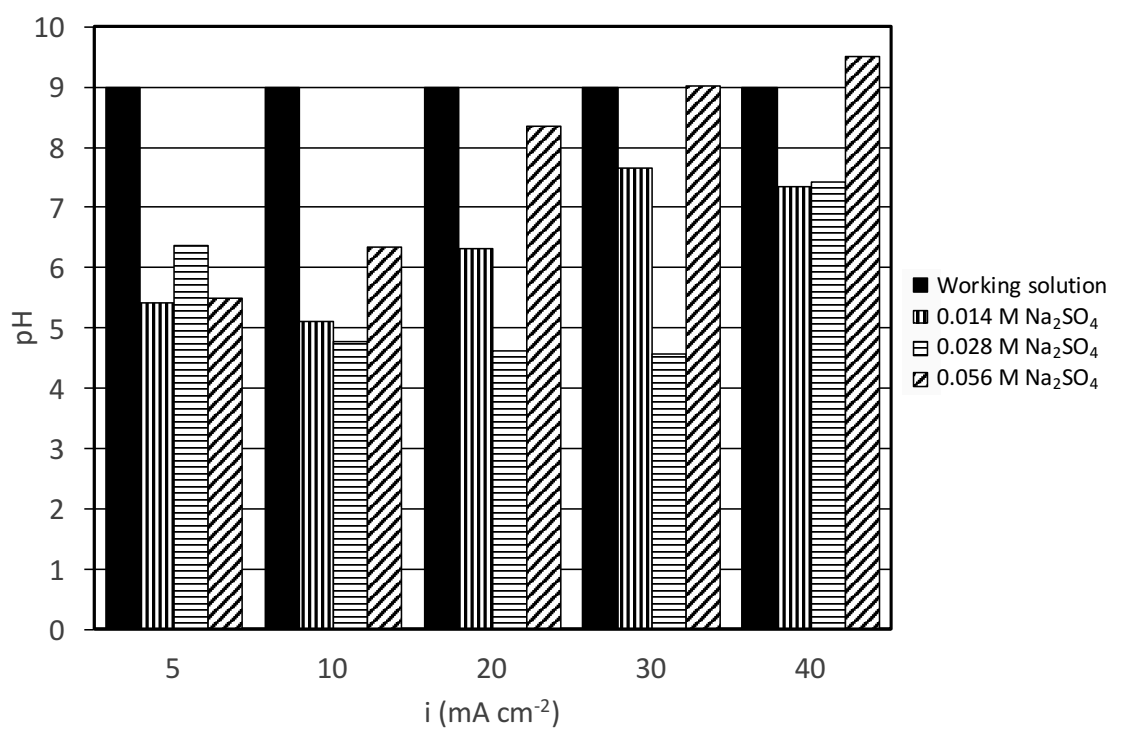
10
9
8
7
6
5
4
3
2
1
0
pH
5
10
20
30
40
i (mA cm-2)
Working solution
0.014 M Na2SO4
0.028 M Na2SO4
0.056 M Na2SO4

Supplementary material for manuscript CHEM60807

Study of the atenolol degradation using a Nb/BDD electrode in a filter-press reactor

Alan Nelson Arenhart Heberle[a,b], Montserrat García-Gabaldón[a], Emma María Ortega[a], Andréa Moura Bernardes[b], Valentín Pérez-Herranz[a*]

[a] Grupo IEC, Departamento de Ingeniería Química y Nuclear, E.T.S.I. Industriales, Universitat Politècnica de València, P.O. Box 22012, E-46071, Valencia, Spain

[b] Universidade Federal do Rio Grande do Sul (UFRGS) – Programa de Pós-Graduação em Engenharia de Minas, Metalúrgica e de Materiais (PPGE3M), Av. Bento Gonçalves, 9500, Porto Alegre/RS, Brazil

*Corresponding author: vperez@iqn.upv.es

Table SM-1. Kinetic parameters for ATL degradation.

$[SO_4^{2-}]$ (M)	i (mA cm^{-2})	k_{zero} (mol L^{-1} min^{-1})	k_{1st} (min^{-1})
0.014	5	7.1×10^{-7}	
	10	1.0×10^{-6}	
	20	1.4×10^{-6}	
	30	3.5×10^{-6}	2.2×10^{-2}
	40		2.5×10^{-2}
0.028	5	8.6×10^{-7}	
	10	1.1×10^{-6}	
	20	1.6×10^{-6}	1.1×10^{-2}
	30	2.1×10^{-6}	1.5×10^{-2}
	40	2.8×10^{-6}	1.9×10^{-2}
0.056	5	1.2×10^{-6}	
	10		
	20	2.6×10^{-6}	3.2×10^{-2}
	30	3.3×10^{-6}	4.5×10^{-2}
	40	4.5×10^{-6}	3.8×10^{-2}

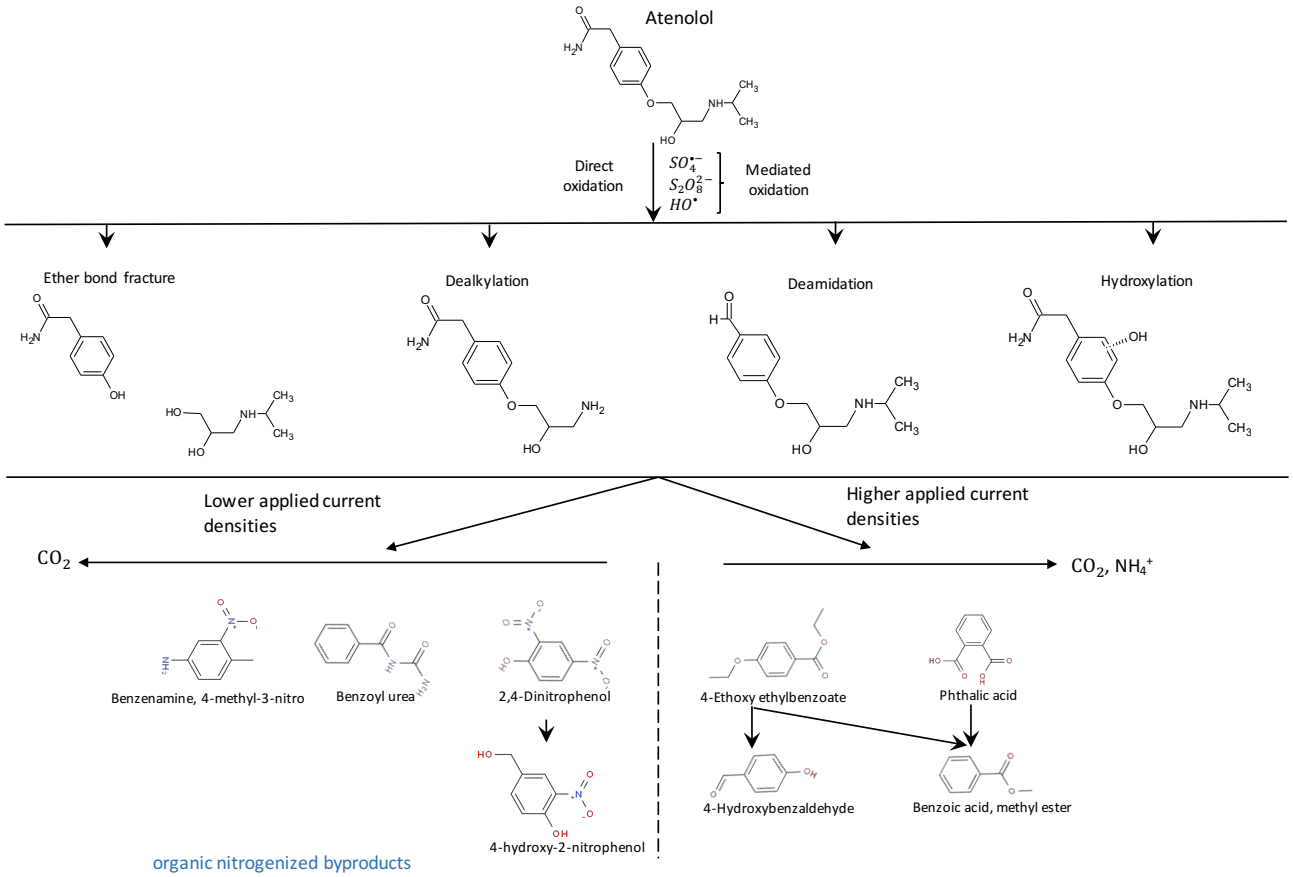

Fig. SM-1. Simplified pathway proposed for ATN degradation.

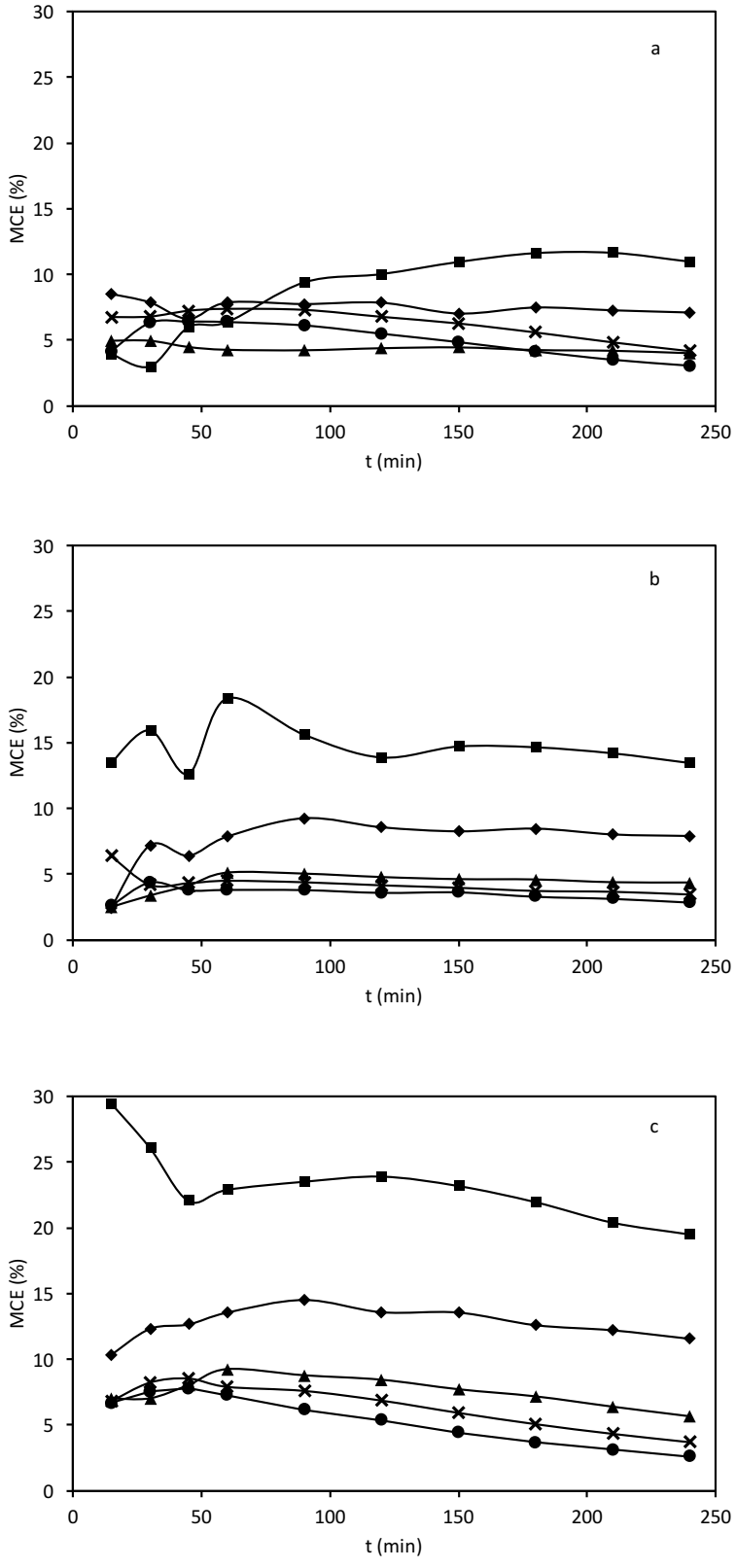

Fig. SM-2. Effect of the applied current density on the mineralization current efficiency. 5 mA cm^{-2} (■), 10 mA cm^{-2} (♦), 20 mA cm^{-2} (▲), 30 mA cm^{-2} (×) and mA cm^{-2} (●). 0.38 mM ATL + 0.014 M Na_2SO_4 (a), 0.028 M Na_2SO_4 (b) and 0.056 M Na_2SO_4 (c).